Observation of dynamic Stark resonances in strong-field excitation

D. Chetty [1,*] R. D. Glover [1,2] B. A. deHarak [1,3] X. M. Tong [4] H. Xu,[1] T. Pauly,[5] N. Smith,[5] K. R. Hamilton [5]
K. Bartschat [5] J. P. Ziegel,[3] N. Douguet,[6] A. N. Luiten,[2] P. S. Light [2] I. V. Litvinyuk,[1] and R. T. Sang [1,†]

[1]*Centre for Quantum Dynamics, Griffith University, Brisbane, Queensland 4111, Australia*
[2]*Institute for Photonics and Advanced Sensing and School of Physical Sciences,*
The University of Adelaide, Adelaide, South Australia 5005, Australia
[3]*Physics Department, Illinois Wesleyan University, Bloomington, Illinois 61702-2900, USA*
[4]*Center for Computational Sciences, University of Tsukuba, 1-1-1 Tennodai, Tsukuba, Ibaraki 305-8573, Japan*
[5]*Department of Physics and Astronomy, Drake University, Des Moines, Iowa 50311, USA*
[6]*Department of Physics, Kennesaw State University, Marietta, Georgia 30060, USA*

We investigate AC Stark-shifted resonances in argon with ultrashort near-infrared pulses. Using 30 fs pulses, we observe periodic enhancements of the excitation yield in the intensity regions corresponding to the absorption of 13 and 14 photons. By reducing the pulse duration to 6 fs with only a few optical cycles, we also demonstrate that the enhancements are significantly reduced beyond what is measurable in the experiment. Comparing these to numerical predictions, which are in quantitative agreement with experimental results, we find that even though the quantum state distribution can be broad, the enhancements are largely due to the efficient population of a select few AC Stark-shifted resonant states rather than the closing of an ionization channel. Because these resonances are dependent on the frequency and intensity of the laser field, the broad bandwidth of the 6 fs pulses means that the resonance condition is fulfilled across a large range of intensities. This is further exaggerated by volume-averaging effects, resulting in excitation of the $5g$ state at almost all intensities and reducing the apparent magnitude of the enhancements. For 30 fs pulses, volume averaging also broadens the quantum state distribution, but the enhancements are still large enough to survive. In this case, selectivity of excitation to a single state is reduced below 25% of the relative population. However, an analysis of time-dependent Schrödinger equation simulations indicates that excitation of up to 60% into a single state is possible if volume averaging can be eliminated and the intensity can be precisely controlled.

I. INTRODUCTION

Strong-field excitation occurs when the interaction of an atom with an intense laser field results in excitation into higher-energy states. In noble gases, a significant portion of these states decay into long-lived metastable states [1,2]. These states have unique properties that enable diverse applications, such as atom lithography [3], radiometric dating by way of atom-trap trace analysis [4,5], and precision measurements in beta decay [6,7]. In recent years, there has been a demand for higher efficiency and cleaner sources of metastable atoms, encouraging all-optical methods of generation to be pursued. Examples include two-photon absorption [8] or methods employing UV lamps [9]. Strong-field excitation is also a promising technique. However, efficient excitation schemes need to be developed to compete with current metastable-generation methods.

In strong laser fields, excitation rates exhibit a complex dependence on the laser intensity, showing distinct enhancements at specific intensities dependent on the target atom [10–12]. The intense electric field of the laser modifies the energy levels of the atom due to the AC (or dynamic) Stark shift [13], resulting in resonances and thresholds at which excitation yields may increase [14–23]. For example, the modification of narrow features in the photoelectron spectra or unexpected changes in the ionization yield at select intensities have been observed and explained through Freeman resonances [24,25], "channel closing" [17,18], and "population trapping" [26–28].

When the laser frequency ω is lower than the frequency of the transition between the ground state and the first-excited state, the ground-state energy drops by $-\alpha_0 I/4$, where I is the laser intensity and α_0 is the static polarizability of the atom (atomic units are used throughout). The continuum threshold, on the other hand, increases with the intensity-dependent ponderomotive energy of the electron, $U_p = I/4\omega^2$ [13]. Together these shifts can exceed the energy of a single photon, thus increasing the number of photons required for photoionization from N to $N + 1$. At this point, the N-photon ionization channel is said to close, thereby providing the condition for an N-photon channel closing as

$$N\hbar\omega = I_p + \frac{I}{4}\left(\frac{1}{\omega^2} + \alpha_0\right), \tag{1}$$

where I_p is the field-free ionization potential. The AC Stark effect also shifts the energy levels of the excited states. For states with a binding energy much less than the ground state, this

---

shift closely follows the continuum threshold. Therefore, as the N-photon ionization channel closes, high-lying Rydberg states are expected to come into resonance. As the intensity increases further, lower-lying states will subsequently shift into resonance. If these states defy ionization from the remaining cycles of the laser pulse, for example through stabilization [29–31], their population may accumulate through population trapping.

In experiments investigating above-threshold ionization, these resonance features in argon photoelectron spectra were found to strongly depend on the laser intensity [32]. Soon after this observation, several theoretical papers were published [20–22,33] detailing that the strong intensity dependence is due to low-lying excited states shifting into resonance with N-photon absorption. Hart *et al.* [34] extended this technique to sodium atoms, demonstrating enhanced ionization at a specific intensity that corresponds to a Freeman resonance for three-photon absorption into the Stark-shifted $5p$ state. These studies, however, did not include the impact on total excitation rates, which is central to the aims of the present investigation.

A recent experiment demonstrated the resultant impacts by directly observing the excitation yields of argon using 45 fs pulses centered at 400 nm [12]. An increase of more than an order of magnitude was observed at the six-photon channel closing. The same experiment with 800 nm pulses, however, could not resolve any enhancements, even though calculations predict them to persist. Extending this, an even more recent experiment [35] appeared to resolve these peak structures in strong-field excitation of xenon with 50 fs pulses centered at 800 nm. In this experiment, a field-ionization technique was employed to detect any excited xenon atoms with principal quantum number $20 < n < 30$. Small features were observed in the ratio of field-ionized neutrals to singly ionized xenon that were attributed to the remainder of the peak structure after focal volume averaging.

In this paper, we present experiments probing strong-field excitation of argon with 30 and 6 fs FWHM pulses centered at 800 nm with intensities between the multiphoton and tunneling regimes, remaining below the barrier throughout. In particular, we focus on the intensities where enhancements are predicted to be most pronounced based on time-dependent Schrödinger equation (TDSE) calculations. By directly detecting excited states, we observe these enhancements experimentally and demonstrate that they are no longer visible for few-cycle pulses. The intensities at which these enhancements occur, as well as an analysis of the nl quantum state distributions predicted by the TDSE, show that the enhancements are due to population trapping rather than the closing of an ionization channel.

II. EXPERIMENTAL PROCEDURE

We directly detect surviving excited Ar atoms after interacting with ultrashort pulses centered at 800 nm with intensities between 70 and 250 TW/cm^2. The apparatus is depicted in Fig. 1. We use a commercially available (Femto Power) laser system to generate 30 fs pulses. Optionally, these pulses can be further compressed using a hollow core fiber to generate 6 fs pulses. The intensity is varied by attenuating the pulse energy using a combination of numerous thin-membrane
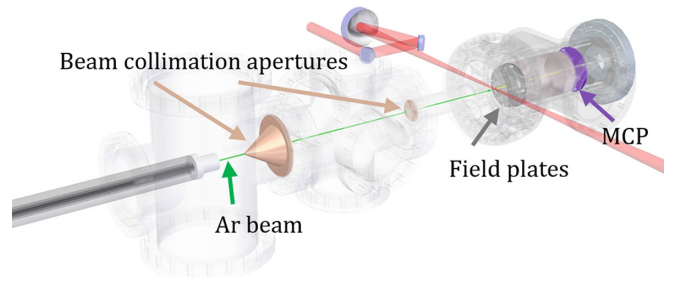

FIG. 1. Scheme of the experimental setup. Linearly polarized laser pulses with duration of either 6 or 30 fs (FWHM) centered at 800 nm are focused into a collimated effusive argon atomic beam. The atomic beam is collinear with a time-of-flight apparatus backed by a microchannel plate (MCP) that allows the identification of particles. The ions are accelerated and temporally separated from the excited neutrals, which remain at thermal speeds. See text for details.

pellicle beam splitters in order to preserve the broadband spectrum and chirp of the pulses. These are then focused and crossed with a 500-μm-wide thermal argon atomic beam. A time-of-flight apparatus collinear with the atomic beam and a microchannel plate (MCP) detector are used to discriminate different particles. Ions are accelerated by the electric fields and detected within a few tens of microseconds, while excited neutral atoms Ar* remain at thermal speeds and arrive in a 0.15–0.6 ms window. These excited states may decay to the long-lived metastable states $(3p^54s)^3P_{2,0}$ during the flight and are directly detected after Penning ionization on the MCP surface due to their high internal energy (>11eV) [36].

III. THEORETICAL METHODS

For the numerical simulations, we solve the TDSE in the single-active-electron (SAE) approximation with the model potential given in Ref. [37]. The radial space is discretized in a generalized pseudospectral grid [38] and the time-dependent wave function is propagated by the second-order split-operator method [39]. We separate the finite box into an inner and outer region to avoid unphysical reflection from the boundary. When the time-dependent wave function propagates into the outer region, we project the wave function onto momentum space to extract the ionization information and then remove it from the wave function in real space, as discussed in [40]. The final ionization probabilities are obtained by integrating the electron momentum distribution over the entire momentum space. After the pulse, we project the inner-region wave function on the field-free atomic excited states to get the nl quantum state population up to $n = 22$, $l = 21$. Summing over all these populations, we obtain the total excitation probability, $P(\text{Ar}^*)$.

The results from the procedure outlined above were compared to independent calculations [41,42] using the same and other similar SAE potentials, such as those suggested in [43] or generated *ab initio* from structure codes such as [44]. The predictions from the various calculations agree to within 5% at lower intensities and 15% at higher intensities when the same potential is used. As expected, the deviations are somewhat larger for different potentials, but qualitatively the agreement remains satisfactory.
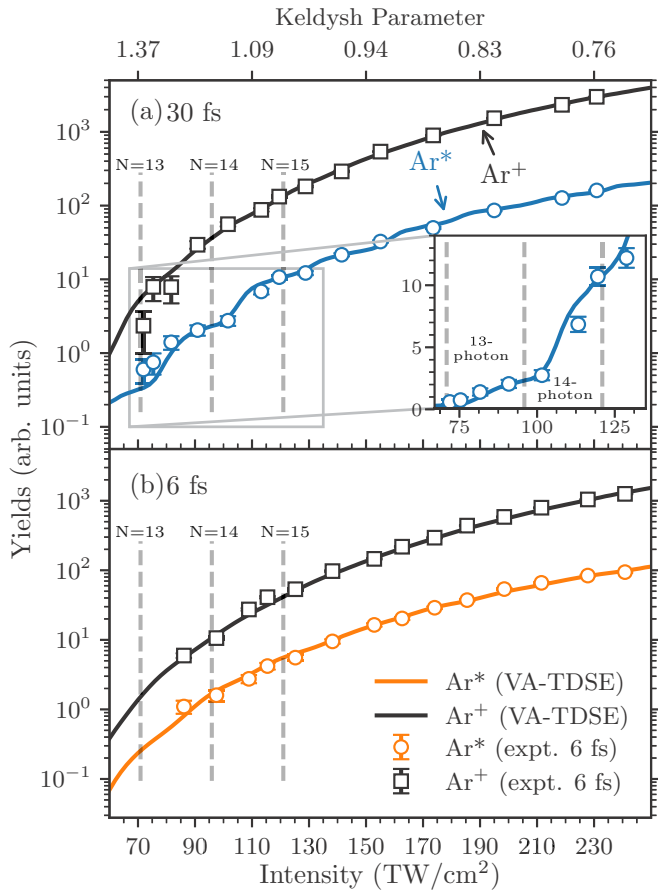
FIG. 2. Yields of singly ionized (black) and excited Ar atoms, Ar*, as a function of laser intensity for (a) 30 fs and (b) 6 fs laser pulses. The solid lines represent the results of the volume-averaged TDSE simulations and include CEP averaging for the 6 fs pulses. The Keldysh parameter is shown above the upper x axis. The zoomed inset shows the region between the 13- and 15-photon channel closings, corresponding to resonances with 13- and 14-photon absorption where a clear modulation is observed for excitation with 30 fs pulses.

To directly compare with experiment, we volume average (VA) the theoretical probabilities to account for the intensity distribution around the laser focus as in Ref. [12]. Since the carrier envelope phase (CEP) of the 6 fs pulse is not stabilized in the experiments, the calculations were averaged over four CEP values from 0 to π in steps of $\frac{\pi}{4}$. The experimental intensity for the 6 fs data was calibrated by fitting the ion yield to a phenomenological model [45]. For the 30 fs data, a two-step process is implemented. The intensity was initially estimated by fitting the ion yield to the ionization rates predicted by an analytical nonadiabatic model for ionization [46], resulting in an uncertainty in the intensity of less than 11%. The initial step is necessary to establish an estimated intensity with an uncertainty less than the channel-closing interval. This allows us to align the experimentally measured peaks to the correct channel. We then fit the Ar* yields to the VA-TDSE results (solid lines in Fig. 2) with constrained parameters from step 1 to obtain a more accurate calibrated intensity ($\pm2\%$). As a consistency check, this fitting procedure was repeated for ionization rates from the TDSE results. This produced a

calibration factor in agreement with the fit to excitation rates within the uncertainty. With this method, the location of the enhancements provides excellent markers for calibrating the experimental intensity [12].

IV. RESULTS AND DISCUSSION

Figure 2 shows the experimental yields of Ar$^+$ (squares) and Ar* (circles) as a function of the calibrated intensity for 30 fs [Fig. 2(a)] and 6 fs [Fig.2(b)] pulses. Within the experimental uncertainty, the observed ionization yields exhibit a monotonous increase with increasing intensity. However, with 30 fs pulses, some features are clearly visible in the metastable yield, which are washed out for 6 fs pulses. We observe good agreement between the experimental data and the VA-TDSE calculations. In particular, the features in the Ar* yields at the 13- and 14-photon absorption channels are well reproduced.

In order to determine the nature of these features, we further analyze the results from the VA-TDSE calculations (see Supplemental Material [47]). We note that the features in the 13- and 14-photon absorption channels with 30 fs pulses appear near intensities where the AC Stark effect shifts the $5g$ ($86\,\mathrm{TW/cm^2}$) and $6h$ ($110\,\mathrm{TW/cm^2}$) states into strongest resonance, respectively. However, due to VA effects, the distribution of quantum states is still relatively broad, with the resonant state accounting for only 17% and 21% of the total population. As a general trend, we see that while the spread of the quantum state distribution varies widely across intensities, the most populated states remain the $6h$, $7h$, and $8h$ states from the 14-photon channel onwards. Similarly, the spread in quantum state distribution varies for the 6 fs pulses, but the most populated state remains at the $5g$ state for all intensities higher than $82\,\mathrm{TW/cm^2}$. Resonances with some of these states were already predicted (see, for example, Ref. [33]), but here we demonstrate that their influence on excitation rates is strong enough to be directly measured in our experiment even after VA and experimental instabilities. This is further evidence that the AC Stark effect has a significant influence on excitation rates—not only in regards to channel closings, which have been linked to similar features previously, but also due to shifted resonances.

The VA results include contributions from lower intensities that wash out or obscure patterns, making it difficult to distinguish whether channel closings or resonances are the cause of these enhancements. The results of the TDSE calculations without VA provide a useful tool for distinguishing these processes and are shown in Fig. 3. The numbers displayed above the upper x axis correspond to the number of absorbed photons required for excitation into that channel. Successive channel closings occur at $\sim26\,\mathrm{TW/cm^2}$ intervals for 800 nm photons and are marked with vertical dashed lines. The general trend is as expected, exhibiting clear enhancements with a periodicity equal to the photon-energy separation. For 30 fs pulses, the enhancements are more pronounced at lower intensities, reaching more than an order of magnitude in the 13- and 14-photon absorption channels, consistent with the findings reported in Ref. [12]. These particular enhancements are significant and are observed under our experimental conditions. For 6 fs pulses, the enhancements are less pronounced and not resolved experimentally due to VA effects. For both pulse
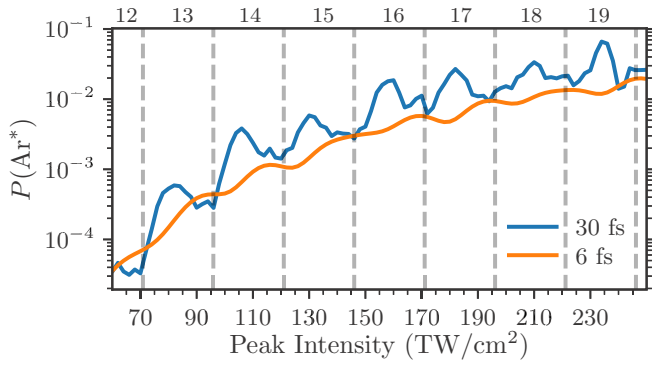
FIG. 3. TDSE calculations for the total excited-state probability, $P(Ar^*)$, for 30 fs pulses in blue (darker line) and 6 fs pulses in orange (lighter line) without volume averaging. The numbers above the upper x axis correspond to the number of absorbed photons resulting in excitation within that channel. The dashed lines indicate the intensities at which an ionization channel closes.

durations, the enhancements occur at higher intensities than the predicted channel closings (at $\sim$12 and $\sim$22 TW/cm^2 for 30 and 6 fs pulses, respectively), indicating that resonances rather than channel closings are the origin of these features.

In order to confirm this interpretation, we first validate that channel closings occur at the predicted intensities by analyzing the relative populations of the quantum angular momentum, l, for each intensity. This is done by summing the nl populations over all n and then scaling to the total probability for excitation at that intensity (from Fig. 3). The distribution in l exhibits parity, preferentially exciting even or odd states due to the dipole selection rules [48]. This has been
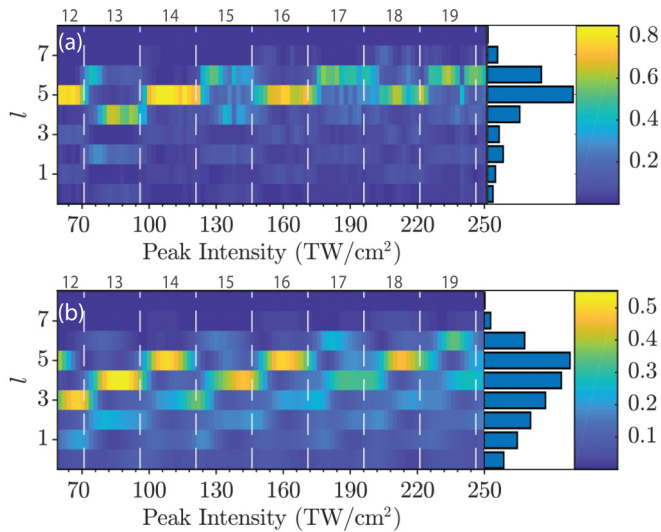

FIG. 4. Relative l distributions found by summing over $n \leqslant 22$ for (a) 30 fs and (b) 6 fs pulses without volume averaging. The numbers above the upper x axis correspond to the number of absorbed photons resulting in excitation within that channel. The bar graphs represent the distribution in l summed across all intensities. For both pulse durations, the l distribution clearly alternates between even and odd parity at the closure of successive ionization channels, providing evidence that an additional photon has been absorbed.
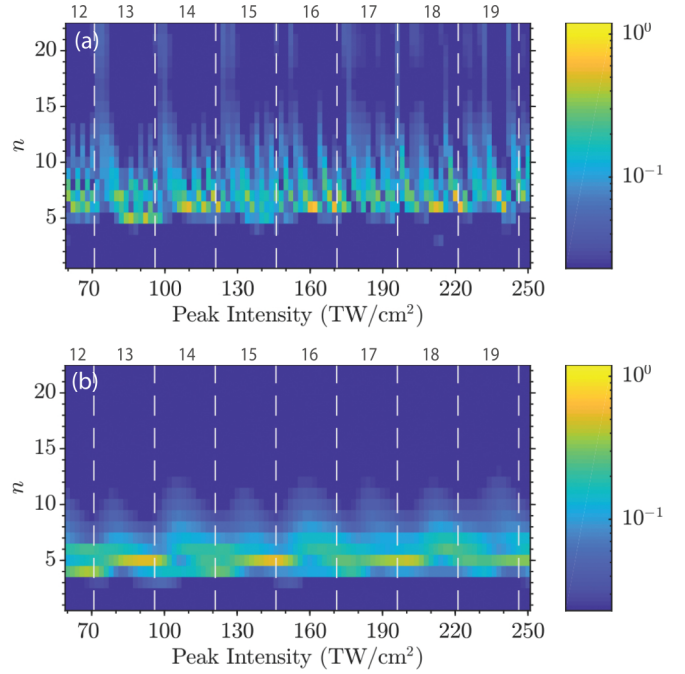

FIG. 5. Relative n populations for (a) 30 fs and (b) 6 fs pulses without volume averaging. The numbers above the upper x axis correspond to the number of absorbed photons resulting in excitation within that channel. The dashed lines indicate the intensities at which an ionization channel closes. High-n states are excited at the channel-closing intensities, shifting to individual resonances with the $6h$ (for 30 fs pulses) and $5g$ state (for both) as the intensity is increased further.

previously studied both semiclassically [49] and quantum mechanically [10,11,35,50]. In argon, which has a $3p$ ($l = 1$) outermost electron in the ground state, the absorption of an even (odd) number of photons will preferentially populate odd (even) l's. This is clearly observed in the l distributions shown in Fig. 4 for both pulse durations, particularly at lower intensities. The change in parity at successive channel-closing intensities is consistent with the condition that one more photon is absorbed, thus confirming the calculated channel-closing locations.

Additionally, for 30 fs pulses, we observe that the population distribution is localized with excitation into $l = 5$ dominating (cf. the bar graph in Fig. 4). For 6 fs pulses, the most populated states remain at $l = 5$, but now the distribution is broadened by excitation into lower-l states.

We now look to at the relative n populations to analyze the patterns around channel closings. These are obtained in a similar procedure as the relative l populations, except by summing over l rather than n; see Fig. 5. In addition, we correlate these observations with those in Fig. 4 for a complete description of the excited-state distribution. See, also, the Supplemental Material for joint-nl distributions [47]. For 30 fs pulses [cf. Fig. 5(a)], a broad range of high-lying excited states ($n \geqslant 12$) is populated shortly after the channel-closing intensity as the AC Stark effect shifts the Rydberg quasicontinuum into resonance. For 6 fs pulses [cf. Fig. 5(b)], the pattern is much the same but not as obvious. This is because the pulse duration is now short compared to the Keppler orbit

periods of high-lying Rydberg states, which are therefore not populated as efficiently [15]. As the intensity increases further, the distribution narrows until a strong resonance with either the $5g$ (for both pulse durations) or $6h$ (for 30 fs) state is reached.

The behavior of this resonance is markedly different for the two pulse durations. First, the intensities at which the strongest resonances are reached in successive channels are different. For example, with 30 fs pulses, the strongest resonance in the 13- and 14-photon absorption channels is reached with the $5g$ and $6h$ states at 86 and 110 TW/cm^2, respectively. On the other hand, with 6 fs pulses, it is reached at 90 and 122 TW/cm^2. Second, the resonances are less dominant and occur over a wider range of intensities for 6 fs pulses compared to 30 fs pulses due to the larger bandwidth enabling resonances over a wider range of photon energies. For example, with 30 fs pulses at 162 TW/cm^2, the $6h$ state accounts for almost 60% of total excitation, but then drops close to zero only 4 TW/cm^2 higher. In comparison, for 6 fs pulses, resonance with the $5g$ state occurs in a 12 TW/cm^2 intensity range, accounting for over 30% of the relative population, peaking at 146 TW/cm^2 with 35% relative population. This reduced dominance, as well as the larger intensity range where resonance is reached, accounts for the reduced magnitude of the enhancements.

Interestingly, we note that even though the intensities of these strong individual resonances are very close to those corresponding to the enhancements observed in the measurements (Fig. 2) and theoretical yields (Fig. 3), they are not the sole contributors. A detailed analysis of the joint-nl distributions from 30 fs pulses indicates that the main contributions to the peaks of the 13- and 14-photon enhancements originate from AC Stark-shifted resonances with a trio of states with successive n and the same l ($5g$, $6g$, $7g$ and $6h$, $7h$, $8h$, respectively). In the case of 6 fs pulses, excitation into the $5g$ state mainly contributes to the enhancements in odd-photon channels, while a broad distribution contributes to the observed enhancements in even-photon channels, at least in the multiphoton regime where the locations of the enhancements are obvious.

V. SUMMARY

We experimentally observed enhancements in excitation rates of Ar for 30 fs pulses centered at 800 nm, which were not present for few-cycle pulses of 6 fs duration. TDSE calculations support the existence of these enhancements even after focal-volume averaging. Due to the sensitivity of these enhancements to intensity changes, they serve as convenient markers for accurate calibration of the experimental intensity. Analysis of the TDSE predictions shows that the enhancements are due to resonant population trapping in a select few states, rather than the closing of an ionization channel. Volume-averaging effects suppress the relative populations of these states at resonant intensities. However, TDSE calculations predict that the resonances are particularly strong for select intensities when using 30 fs pulses, but spread over a larger intensity range for 6 fs pulses due to the large bandwidth of the pulse. In the future, enhanced excitation of the $5g$ and $6h$ states might be exploited as a means to increase metastable yields by directly stimulating them into the metastable state.

[1] T. Nubbemeyer, K. Gorling, A. Saenz, U. Eichmann, and W. Sandner, Phys. Rev. Lett. **101**, 233001 (2008).

[2] H. Zimmermann, J. Buller, S. Eilzer, and U. Eichmann, Phys. Rev. Lett. **114**, 123003 (2015).

[3] M. Baker, A. J. Palmer, W. R. MacGillivray, and R. T. Sang, Nanotechnology **15**, 1356 (2004).

[4] Z.-T. Lu, P. Schlosser, W. Smethie, N. Sturchio, T. Fischer, B. Kennedy, R. Purtschert, J. Severinghaus, D. Solomon, T. Tanhua *et al.*, Earth-Sci. Rev. **138**, 196 (2014).

[5] N. C. Sturchio, K. L. Kuhlman, R. Yokochi, P. C. Probst, W. Jiang, Z.-T. Lu, P. Mueller, and G.-M. Yang, J. Contam. Hydrol. **160**, 12 (2014).

[6] A. Knecht, Z. Alexander, Y. Bagdasarova, T. M. Cope, B. Delbridge, X. Fléchard, A. García, R. Hong, E. Liénard, P. Mueller *et al.*, in *11th Conference on the Intersections of Particle and Nuclear Physics: (CIPANP 2012)*, edited by B. Fleming, AIP Conf. Proc. No. 1560 (AIP, New York, 2013), p. 636.

[7] B. Ohayon, J. Chocron, T. Hirsh, A. Glick-Magid, Y. Mishnayot, I. Mukul, H. Rahangdale, S. Vaintraub, O. Heber, D. Gazit *et al.*, Hyperfine Interact. **239**, 57 (2018).

[8] M. A. Dakka, G. Tsiminis, R. D. Glover, C. Perrella, J. Moffatt, N. A. Spooner, R. T. Sang, P. S. Light, and A. N. Luiten, Phys. Rev. Lett. **121**, 093201 (2018).

[9] M. Kohler, H. Daerr, P. Sahling, C. Sieveke, N. Jerschabek, M. B. Kalinowski, C. Becker, and K. Sengstock, Europhys. Lett. **108**, 13001 (2014).

[10] Q. Li, X.-M. Tong, T. Morishita, H. Wei, and C. D. Lin, Phys. Rev. A **89**, 023421 (2014).

[11] B. Piraux, F. Mota-Furtado, P. F. O'Mahony, A. Galstyan, and Y. V. Popov, Phys. Rev. A **96**, 043403 (2017).

[12] H. Zimmermann, S. Patchkovskii, M. Ivanov, and U. Eichmann, Phys. Rev. Lett. **118**, 013003 (2017).

[13] N. B. Delone and V. P. Krainov, Phys. Usp. **42**, 669 (1999).

[14] R. R. Freeman, P. H. Bucksbaum, H. Milchberg, S. Darack, D. Schumacher, and M. E. Geusic, Phys. Rev. Lett. **59**, 1092 (1987).

[15] F. Grasbon, G. G. Paulus, H. Walther, P. Villoresi, G. Sansone, S. Stagira, M. Nisoli, and S. De Silvestri, Phys. Rev. Lett. **91**, 173003 (2003).

[16] A. Rudenko, K. Zrost, C. Schröter, V. De Jesus, B. Feuerstein, R. Moshammer, and J. Ullrich, J. Phys. B: At. Mol. Opt. Phys. **37**, L407 (2004).

[17] P. Kruit, J. Kimman, H. G. Muller, and M. J. V. der Wiel, J. Phys. B **16**, 937 (1983).

[18] H. G. Muller, A. Tip, and M. J. van der Wiel, J. Phys. B **16**, L679 (1983).

[19] H. G. Muller, Phys. Rev. Lett. **83**, 3158 (1999).

[20] H. G. Muller, Phys. Rev. A **60**, 1341 (1999).

[21] M. J. Nandor, M. A. Walker, L. D. Van Woerkom, and H. G. Muller, Phys. Rev. A **60**, R1771(R) (1999).

[22] H. G. Muller and F. C. Kooiman, Phys. Rev. Lett. **81**, 1207 (1998).

[23] M. Li, P. Zhang, S. Luo, Y. Zhou, Q. Zhang, P. Lan, and P. Lu, Phys. Rev. A **92**, 063404 (2015).

[24] R. R. Freeman and P. H. Bucksbaum, J. Phys. B: At., Mol. Opt. Phys. **24**, 325 (1991).

[25] R. M. Potvliege and S. Vučić, J. Phys. B: At., Mol. Opt. Phys. **42**, 055603 (2009).

[26] M. P. de Boer and H. G. Muller, Phys. Rev. Lett. **68**, 2747 (1992).

[27] R. R. Jones, D. W. Schumacher, and P. H. Bucksbaum, Phys. Rev. A **47**, R49(R) (1993).

[28] T. Morishita and C. D. Lin, Phys. Rev. A **87**, 063405 (2013).

[29] E. A. Volkova, A. M. Popov, and O. V. Tikhonova, J. Expt. Theor. Phys. **113**, 394 (2011).

[30] A. M. Popov, O. V. Tikhonova, and E. A. Volkova, J. Phys. B: At., Mol. Opt. Phys. **36**, R125(R) (2003).

[31] S. L. Chin and H. Xu, J. Phys. B: At., Mol. Opt. Phys. **49**, 222003 (2016).

[32] M. P. Hertlein, P. H. Bucksbaum, and H. G. Muller, J. Phys. B: At. Mol. Opt. Phys. **30**, L197 (1997).

[33] H. Muller, Opt. Express **8**, 44 (2001).

[34] N. A. Hart, J. Strohaber, A. A. Kolomenskii, G. G. Paulus, D. Bauer, and H. A. Schuessler, Phys. Rev. A **93**, 063426 (2016).

[35] S. Hu, X. Hao, H. Lv, M. Liu, T. Yang, H. Xu, M. Jin, D. Ding, Q. Li, W. Li *et al.*, Opt. Express **27**, 31629 (2019).

[36] F. Penent, P. Lablanquie, R. I. Hall, M. Žitnik, K. Bučar, S. Stranges, R. Richter, M. Alagia, P. Hammond, and J. G. Lambourne, Phys. Rev. Lett. **86**, 2758 (2001).

[37] X. M. Tong and C. D. Lin, J. Phys. B: At. Mol. Opt. Phys. **38**, 2593 (2005).

[38] X.-M. Tong and S.-I. Chu, Chem. Phys. **217**, 119 (1997).

[39] A. D. Bandrauk and H. Shen, J. Chem. Phys. **99**, 1185 (1993).

[40] X. M. Tong, K. Hino, and N. Toshima, Phys. Rev. A **74**, 031405(R) (2006).

[41] E. V. Gryzlova, A. N. Grum-Grzhimailo, E. I. Staroselskaya, N. Douguet, and K. Bartschat, Phys. Rev. A **97**, 013420 (2018).

[42] A. C. Brown, G. S. Armstrong, J. Benda, D. D. Clarke, J. Wragg, K. R. Hamilton, Z. Mašín, J. D. Gorfinkiel, and H. W. van der Hart, Comput. Phys. Commun. **250**, 107062 (2020).

[43] A. E. S. Green, D. L. Sellin, and A. S. Zachor, Phys. Rev. **184**, 1 (1969).

[44] W. Eissner, M. Jones, and H. Nussbaumer, Comput. Phys. Commun. **8**, 270 (1974).

[45] W. C. Wallace, O. Ghafur, C. Khurmi, S. Sainadh U, J. E. Calvert, D. E. Laban, M. G. Pullen, K. Bartschat, A. N. Grum-Grzhimailo, D. Wells *et al.*, Phys. Rev. Lett. **117**, 053001 (2016).

[46] M. Li, J.-W. Geng, M. Han, M.-M. Liu, L.-Y. Peng, Q. Gong, and Y. Liu, Phys. Rev. A **93**, 013402 (2016).

[47] See Supplemental Material at http://link.aps.org/supplemental/10.1103/PhysRevA.101.053402 for movies showing the joint-*nl* distributions.

[48] K. Krajewska, I. I. Fabrikant, and A. F. Starace, Phys. Rev. A **86**, 053410 (2012).

[49] D. G. Arbó, K. I. Dimitriou, E. Persson, and J. Burgdörfer, Phys. Rev. A **78**, 013406 (2008).

[50] Z. Chen, T. Morishita, A.-T. Le, M. Wickenhauser, X. M. Tong, and C. D. Lin, Phys. Rev. A **74**, 053405 (2006).